Synthesis of N-((2-hydroxynaphthalen-1-yl) (4-nitrophenyl) methyl)-N-methyl acetamide under solvent free condition, its characterization, antibacterial, antioxidant, computational and docking studies with HIV-1 protein

P. Vivekanandan[1], A. Daniel Aroquiaraj[1], K.S. Satheeshkumar[1]*, Francixavier Paularokiadoss[2*], Bouzid Gassoumi[3] and Sahbi Ayachi[4]

[1]*Department of Chemistry, Arignar Anna Government Arts College, Villupuram - 605602, Affiliated to Thiruvalluvar University, Serkkadu, Velore-632 115, Tamil Nadu, India.*
[2]*PG& Research Department of Chemistry, St. Joseph College of Arts & Science, Cuddalore- 607001, Tamil Nadu, India.*
[3]*Laboratory of Advanced Materials and Interfaces (LIMA), University of Monastir, Faculty of Sciences of Monastir, Avenue of Environment, 5000 Monastir, Tunisia.*
[4]*Laboratory of Physico-Chemistry of Materials (LR01ES19), Faculty of Sciences, University of Monastir, Avenue of the Environment, 5019 Monastir, Tunisia.*

* Corresponding authors: *drkssatheeshkumar@gmail.com; paul_adoss@yahoo.com*

KEYWORDS

2-naphthol derivatives, Density functional theory, Solvent free synthesis, Molecular docking studies, Antibiotic studies and Antioxidant studies.

ABSTRACT

In the present work, a competent and eco-friendly route for the synthesis of N-((2-hydroxynaphthalen-1-yl) (4-nitrophenyl) methyl)-N-methyl acetamide (HNMA) catalyzed by trichloroacetic acid and also using montmorillonite K10 clay under solvent free condition have been described. Thus, synthesized HNMA was characterized for its structure using spectroscopic tools such as UV-Visible, FT-IR, ^{1}H NMR, ^{13}C NMR and QTOF analyses. Under *in vitro* conditions, HNMA was found to exhibit potential antibacterial property against Escherichia coli and Staphylococcus aureus bacteria. In addition to the above, it exhibits excellent antioxidant property which was examined using DPPH radical scavenging capacity assay. Further, computational studies such as the electronic property along with its stability were studied by analyzed HOMO-LUMO gap. To understand charge distribution around HNMA molecule, Molecular Electrostatic Potential (MEP) study was performed which reveal that it has strong interaction with nucleophiles. Theoretical UV-Visible spectral analysis, infers that it has a quite higher optical band gap of 3.51 eV suggesting that HNMA primarily absorb ultraviolet light and appear transparent to visible light. Further structural and electronic properties of HNMA was investigated using infrared spectral study which conclude that it exhibit a strong intramolecular hydrogen bonding. Raman spectra of HNMA was simulated using density functional theory at the B3LYP/6-311G (d,p) level, which support its structure. The experimental ^{1}H and ^{13}C chemical shifts are in excellent agreement with the calculated values. The nonlinear optical (NLO) calculations indicate that it has higher dipole moment and hyperpolarizability. To further understand the nature of intra and intermolecular interactions between atoms and groups, quantum theory of atoms in molecules (QTAIM) analysis was also studied which indicate that the interactions are non-covalent in nature. Finally, docking study was performed to analyze its therapeutic activity against the target protein 1PVG, which is associated with HIV-1.

1. INTRODUCTION

In recent years, one-pot multicomponent reactions (MCRs) have gained recognition as a useful technique for the synthesis of biologically active organic compounds as the product can be generated in a single step with better yield and purity[1]. There has been remarkable development in MCRs over the past few decades involving three or four components[2-4]. However, considerable efforts have been made in recent years to further develop new MCRs[5]. The chemical transformation using MCRs is highly preferred due to its easy handling of reactants, better yield efficiency, no need for excess separation steps and also as it evades the formation of environmental pollutants. One of the catalysts used for the present study is trichloro acetic acid, as it is inexpensive, readily available, requires lesser reaction time, can be conveniently be handled and removed instantly from the reaction mixture after synthesis under solvent-free conditions[6-11]. Another notable catalyst, Montmorillonite K10, is also highly effective due to its stability, eco-sustainability, ease of handling and simple recovery under solvent-free conditions[12-15]. Thus, the remarkable catalytic activities together with their operational simplicity make them the most suitable catalysts for this synthesis[16-19] in contrast to conventional methods which require costly reagents, use of organic solvents, and prolonged reaction durations. These characteristics, along with their significant catalytic activity and simplicity of use, make them ideal catalysts for the synthesis of N-((2-hydroxynaphthalen-1-yl) (4-nitrophenyl) methyl)-N-methyl acetamide from 2-naphthol, nitro benzaldehyde and N-Methyl acetamide (HNMA).

After synthesizing HNMA, it was characterized using suitable spectroscopic tools to confirm their structure and purity. The antibacterial activity of the above compounds was screened against Escherichia coli and Staphylococcus aureus bacteria under in vitro conditions. In recent years, molecules that exhibit both antibacterial and antioxidant activities are attractive candidates to develop new drugs[20,21]. Hence, in addition to antibacterial property, its antioxidant property was also analyzed using DPPH radical scavenging capacity assay.

Recently, the computational work on chemical molecules has exceedingly drawn a lot of attention among researchers and scientists as a means of understanding its complete information about its structure[21]. The intention of computational work in the present study is to investigate the molecular structural information. The study has been complemented by natural bond orbital (NBO) calculations with an analysis of the electron charge transfer through the intramolecular contacts. In addition, the molecular electrostatic potential (MEP), frontier molecular orbital analysis properties were investigated using theoretical calculations. All the calculations done in this work are obtained by DFT/B3LYP method with 6-31G(d,p) basis set.

The knowledge gained from this study can provide information about the design of new molecules with tailored optical and electronic properties. Future studies could focus on introducing other electron-withdrawing or electron-donating substituents to understand their impact comprehensively. Additionally, experimental validation of the simulated spectra is essential to confirm the theoretical predictions and assess the practical applicability of such compound in real-world scenarios, such as their use as UV-absorbing materials and in various biological applications.

2. EXPERIMENTAL SECTION

2.1 Synthesis of HNMA using Trichloroacetic acid (Method A).

A mixture of 2-naphthol (1 mmol), p-nitrobenzaldehyde (1 mmol), N-methyl acetamide (1.5 mmol), and trichloroacetic acid were stirred at 405 K for 64 minutes without the use of any solvent medium. The yield of HNMA thus synthesized was observed to be 80%. Thin-layer chromatography (TLC) was employed to

monitor the progress of reaction in a solvent system of 2:8 ethyl acetate to n-hexane. After completion of reaction, the product was cooled to room temperature, followed by a water wash, and column chromatography assists in obtaining pure product.

2.2 Synthesis of HNMA using Montmorillonite K10 (Method B).

The mixture of N-methyl acetamide (1.5 mmol), p-nitrobenzaldehyde (1 mmol), 2-naphthol (1 mmol), and montmorillonite K10 clay (0.25 g) were combined and agitated at 405 K for 100 min without the use of any solvent medium as in method A. The yield of HNMA thus synthesized was observed to be 61%. The progress of the reaction was tracked using thin-layer chromatography-with a 2:8 ethyl acetate and n-hexane solvent system. Following completion, the mixture was allowed to cool to room temperature, washed with water, and column chromatography was used to separate the finished product into pure component.

2.3. Spectral data of HNMA.

Calculated for $C_{20}H_{18}N_2O_4$: C=68.56%, H=5.18%, N=8.00%, O=18.27%; UV-Visible: 332.5 nm ^{1}H NMR (400 MHz, $CDCl_3$): δ 2.05 (3H, s), 2.87 (3H, s), 6.28 (1H, s), 7.06 (1H, dd, *J* = 8.8Hz), 7.29-7.54 (5H, m), 7.82 (1H, d) *J* = 7.9Hz), 7.95-8.08 (3H, d, *J* = 8.6 Hz). ^{13}C NMR: δ 21.07, 29.7, 111.9, 116.4, 124.2, 125.0, 126.4, 126.5, 127.6, 128.5, 128.5, 128.5, 132.7, 133.8, 135.3, 137.9, 164.4, 168.8; FT-IR (KBr): 3446 cm^{-1} (O-H, aromatic stretching), 3074 cm^{-1} (C-H, aromatic stretching), 1697 cm^{-1} (C=O, amide stretching), 1602–1467 cm^{-1} (C=C, aromatic stretching), 1526 (N-O stretching) 1228 cm^{-1} (C-O/C-N stretching), 825 cm^{-1} (C-H, aromatic, out-of-plane bending); Molecular weight (quadrupole time of flight (QTOF) method): 350.2132 u.

2.4 Antibacterial Study -Using Agar disc diffusion method

In vitro antibacterial activities of HNMA was screened against pathogenic bacteria (Escherichia coli and Staphylococcus aureus) using ampicillin (20µL/disc) as a standard, employing the agar disk diffusion method[22-24]. Stock cultures were maintained on nutrient agar slants at 277 K. In order to begin active cultures for experimental purposes, a loopful of the stock culture was transferred into test tubes filled with nutrient broth, and the tubes were then incubated at 310 K for 24 hours. Muller Hinton agar (MHA) plates were prepared by pouring the medium into Petri dishes, which were then inoculated with bacterial strains at a concentration of 10^8 CFU. For 3 hours, the plates were incubated at 310 K to promote bacterial growth. After the medium solidified, a sterile swab moistened with the bacterial suspension was used to evenly spread the suspension across the agar surface. Sterile discs were placed on the MHA plates, and 20 µL of each sample, at concentrations of 1000, 750, and 500 µg/mL, was applied to the discs. Ampicillin, which served as the standard control, was made using nutrient agar tubes with double-distilled water. The inhibition zone around the discs was measured after incubating at 310 K for 18 to 24 hours. The diameter of these inhibition zones was used to evaluate the antibacterial activity.

2.5 Antioxidant Study - Using Radical Scavenging Method

The synthesized compound HNMA was assessed using the 2,2-Diphenyl-1-picrylhydrazyl (DPPH) radical scavenging method to determine the antioxidant activity[25]. A DPPH (10^{-4} M) methanolic solution was made. Each sample was evaluated in duplicate using 1-mL aliquots at doses of 200, 400, 600, 800, and 1000 µg/mL. To each aliquot, 2 mL of the methanolic DPPH solution was added. DPPH, a stable free radical

with delocalized unpaired electrons, maintains a deep violet colour due to its absorption of around 500 nm in ethanol. The mixture was incubated in the dark at room temperature for 30 minutes; afterwards, a UV-30 spectrophotometer was used to detect absorbance at 520 nm (GIORGIO-BORMAC SRL, Carpi, Italy). The methanolic DPPH solution was the only one used to prepare the blank.

2.6 Minimum Inhibitory Concentration (MIC) Study

MIC is the lowest concentration of an antibacterial agent expressed in µg/mL at which bacterial growth is completely inhibited. 1mg of HNMA was taken and mixed with 1ml of DMSO obtaining the concentration of 1mg/ml. The method of successive dilution was adopted to find the MIC values. 1ml of sterile Lysogeny broth was distributed for every tube and was submitted to autoclave under constant pressure at the temperature of 394 K. After the broth reaches room temperature, 1 ml of diluted sample was added to tube 1. From tube 1, 1 ml was transferred to tube 2 which was repeated successively until tube 8. 100 µl of bacterial cultures were added to all the tubes from 1 to 8. The above was incubated at 310 K for 24 hours. After incubation, the turbidity was observed. MIC is the concentration of higher dilution tubes in which the absence of bacterial growth has occurred.

2.7. Details of computational analysis

The structural properties of the synthesized compounds were initially optimized using hybrid density functional theory (DFT) with the functional B3LYP and a basis set 6-311G (d,p). Following optimization, calculations of the lowest unoccupied molecular orbital (LUMO) energy along with highest occupied molecular orbital (HOMO) energy and the molecular electrostatic potential (MEPs) were also performed to assess the reactivity and band gap of the molecules. All calculations were carried out using Gaussian 09 W software,[26] with results visualized using GaussView.[27] Topological parameters were derived from the quantum theory of atoms in molecules (QTAIM) using the Multiwfn package.[28,29] To further investigate covalent and non-covalent bonding, localized orbital locator (LOL) and electron localization function (ELF) iso-surfaces were analyzed.[30,31]

3. RESULTS AND DISCUSSION

3.1 Synthetic Chemistry

For the reaction of p-nitrobenzaldehyde, 2-naphthol and N-methyl acetamide, the reaction conditions were optimized using TCA as catalyst and also using montmorillonite K10 clay. The yield was found to be 80 % and 61 % for TCA and montmorillonite K10 clay as catalyst respectively. The percentage yield obtained revealed that the best conditions was solvent free at 405 K using catalytic amounts (35 mol %) of TCA. A little extra of the N-methyl acetamide was found to be advantageous and hence the molar ratio of 2-naphthol to N-methyl acetamide was kept at 1:1.5. Thus, HNMA was prepared under the optimized reaction conditions. Under the solvent free condition, reaction was carried out using montmorillonite K10 clay instead of TCA as a catalyst. It is observed that the % yield was good without any by products; however, the yield was not as high as in the case of TCA as catalyst. The proposed mechanism for the TCA catalyzed synthesis of N-((2-hydroxynaphthalen-1-yl) (4-nitrophenyl) methyl)-N-methyl acetamide (HNMA) from the reaction of 2-naphthol, p-nitrobenzaldehyde and N-methyl acetamide is shown in Scheme I. Thus, prepared HNMA is characterized precisely using spectroscopic tools. UV-visible spectrum exhibited a peak at 332.5 nm, which is due to p-nitro phenol chromophore. The number and type of hydrogens and carbons were

characterized using ^{1}H NMR and ^{13}C NMR spectra which were in agreement with literature[32]. Finally, the molecular weight of 350.2132 u which was estimated from QTOF was found to be in agreement with expected value. The structure of HNMA was confirmed in accordance with spectral data.

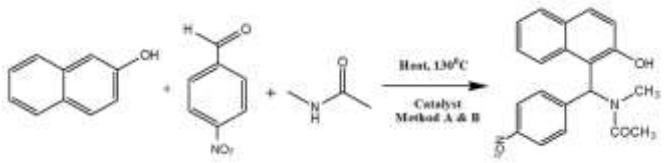

Scheme I. Synthesis of synthesis of N-((2-hydroxynaphthalen-1-yl) (4-nitrophenyl) methyl)-N-methyl acetamide from the reaction of 2-naphthol, p-nitrobenzaldehyde and N-methyl acetamide. Method A is using trichloroacetic acid and method B is using Montmorillonite K-10 as catalyst.

3.2 Antibacterial Studies

The antibacterial activities of HNMA was investigated by using Escherichia coli and Staphylococcus aureus as bacteria samples. The stock solutions used in this study were prepared in DMSO. The increasing resistance of microorganisms to antibiotics makes it necessary to synthesize compounds that can be used as antibiotics[33-34]. The antibacterial activity of HNMA was studied at different concentrations (500, 750 and 1000 µg/ml) against two pathogenic bacteria namely Escherichia coli and Staphylococcus aureus. Antibacterial potential of HNMA was assessed in terms of zone of inhibition of bacterial growth. The results are presented in Table 1 which exhibit HNMA has significant antibacterial effects. Moreover, the antibacterial activity of HNMA increased linearly with increase in concentration (µg/ml). The results reveal HNMA is extremely active against bacterial growth as that of the standard drug ampicillin. The growth inhibition zone measured ranged from 8 to 21 mm for the bacterial strains [Figure 1]. The results show that the HNMA was found to be more effective against Staphylococcus aureus.

Organisms	% inhibition at MIC = 31.2	Zone of Inhibition (in mm)			
		Sample (µg/ml)			Std.
		1000	750	500	
Escherichia coli	20.14	12	10	9	14
Staphylococcus Aureus	30.75	16	14	12	18

Table 1: Antibacterial activities of HNMA against Escherichia coli and Staphylococcus Aureus bacterial test organisms.

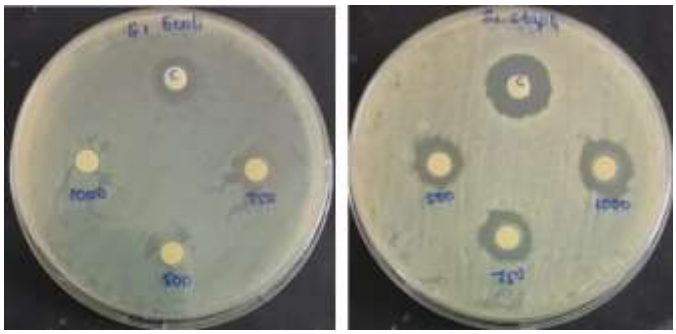

Figure 1: Pictorial display of Antibacterial activities of HNMA against Escherichia coli and Staphylococcus aureus

3.3 Antioxidant Studies

The study of antioxidant activity of various novel synthetic compounds has boomed in recent years[35-37]. When a solution of DPPH is mixed with that of a substance that can donate a hydrogen atom, then this gives rise to the reduced form[38] with the loss of this violet colour (although there would be expected to be a residual pale yellow colour from the picryl group still present). Representing the DPPH radical by Z• and the donor molecule by AH, the primary reaction is: Z• + AH = ZH + A•; where ZH is the reduced form and A• is free radical produced in this first step. This latter radical will then undergo further reactions which control the overall stoichiometry, that is, the number of molecules of DPPH reduced (decolorized) by one molecule of the reductant. Aliquot 3.7 ml of absolute methanol in all test tubes and 3.8ml of absolute methanol was added to blank.

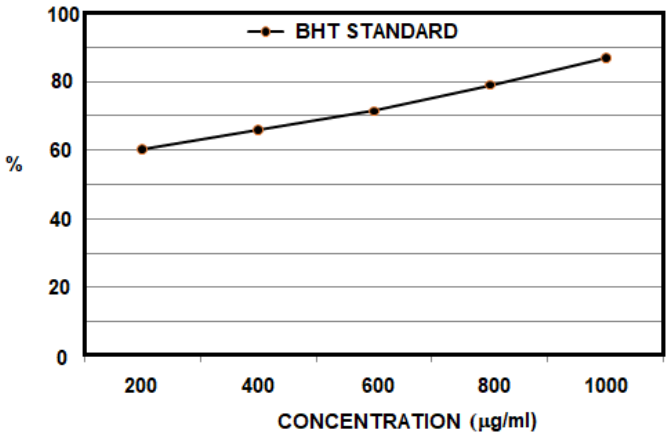

Figure 2: The calibration graph of BHT standard at different concentrations

S.No.	Concentration of HNMA (µg/ml)	Optical density	% DPPH Activity
1	200	0.221	36.85
2	400	0.189	46.00

3	600	0.153	56.28
4	800	0.117	66.57
5	1000	0.079	77.42

Table 2: The % DPPH activity of HNMA at different concentrations along with its optical density values. The optical density of control was found to be 0.430.

100µl of Butylated hydroxyl toluene (BHT) was added to tube marked as standard and 100µl of respective samples to all other tubes marked as tests. 200µl of DPPH reagent was added to all the test tubes including blank. Incubate all test tubes at room temperature in dark condition for 30 minutes. The absorbance of all samples was read at 517nm. The calibration graph is shown in Figure 2 and their % DPPH activity is given in Table 2.The calibration line was established using the following concentrations of BHT: 200, 400, 600, 800 and 1000 µg/mL. The percentage antioxidant activity was measured by taking the ratio of difference between the absorbance values of blank and sample to the absorbance of blank which is multiplied by hundred. The findings of this study also clearly demonstrate that HNMA provide an excellent antioxidant effect.

3.4 Electronic Properties and Stability

To study the optoelectronic and semiconducting property of HNMA, the quantum chemical data were analyzed using the 6-31G (d,p) and 6-311G (d,p) basis sets. The results are depicted in Table 3. Key parameters include Highest Occupied Molecular Orbital (HOMO) and Lowest Unoccupied Molecular Orbital (LUMO) energies (ε_{HOMO} and ε_{LUMO})**,** the electronic band gap (Δ_{H-L})**,** dipole moment**,** and stabilization energy (E_S). The 6-311G(d,p) basis set consistently yields lower ε_{HOMO} and ε_{LUMO} values, a slightly larger Δ_{H-L}, and similar dipole moments compared to 6-31G(d,p), indicating improved accuracy. HNMA is more stable and less reactive (higher Δ_{H-L}). The dipole moments indicate significant polarity, which can influence solubility and intermolecular interactions. These findings are essential for understanding the electronic properties and potential applications of HNMA.

Basis Set	ε_{HOMO} (eV)	ε_{LUMO} (eV)	Δ_{H-L} (eV)	Dipole Moment (Debye)	E_S
6-31 g(d,p)	-5.861	-2.605	3.256	7.029	-1183.323
6-311 g(d,p)	-6.100	-2.786	3.314	7.011	-1183.596

Table 3: Quantum chemical parameters of HNMA using different basis sets.

The nitro (-NO_2) group is a strong electron-withdrawing group that lowers both HOMO and LUMO energies, increasing the HOMO-LUMO gap (Δ_{H-L}) and enhancing stability but reducing conductivity. It also increases the dipole moment and makes the molecule more electrophilic and enhances charge transfer, making such molecules useful in optoelectronics and organic semiconductors.

3.5 Frontier Molecular Orbitals (FMOs) Analysis

To provide insight into the electronic properties and reactivity, FMO analysis were performed on HNMA. The Figure 3 illustrates the HOMO and LUMO frontier molecular orbitals for HNMA. In HNMA, the HOMO is primarily localized on the naphthalene moiety and adjacent nitrogen-containing group, indicating strong π-conjugation, while the LUMO is concentrated on the nitro group and part of the conjugated system, highlighting an electron-withdrawing effect that enhances charge transfer potential. This spatial separation between the HOMO and LUMO indicates significant intramolecular charge transfer (ICT), where electron density shifts from the electron-rich dimethylamino group to the electron-deficient naphthalene and nitrogen-containing group upon excitation.

To analyze the tendency of interaction of HNMA towards electrophiles and nucleophiles, the molecular electrostatic potential (MEP) was studied. The MEP plot illustrate charge distribution in molecular structure of HNMA which is depicted in the third column of Figure 3. The colour scale at the top ranges from red (electron-rich, partially negative regions) to blue (electron-deficient, partially positive regions), with green and white representing neutral or intermediate regions. For HNMA, a strong blue region indicates a highly positive electrostatic potential, likely due to an electron-deficient site such as a protonated nitrogen or an electrophilic group. Consequently, the HNMA may have stronger interactions with nucleophiles or participate in different intermolecular interactions**.**

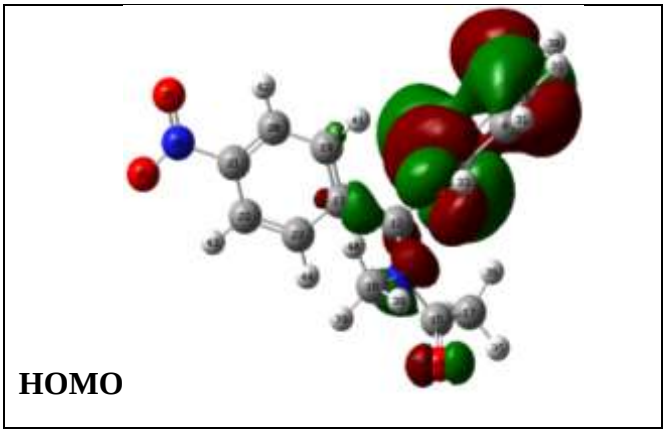

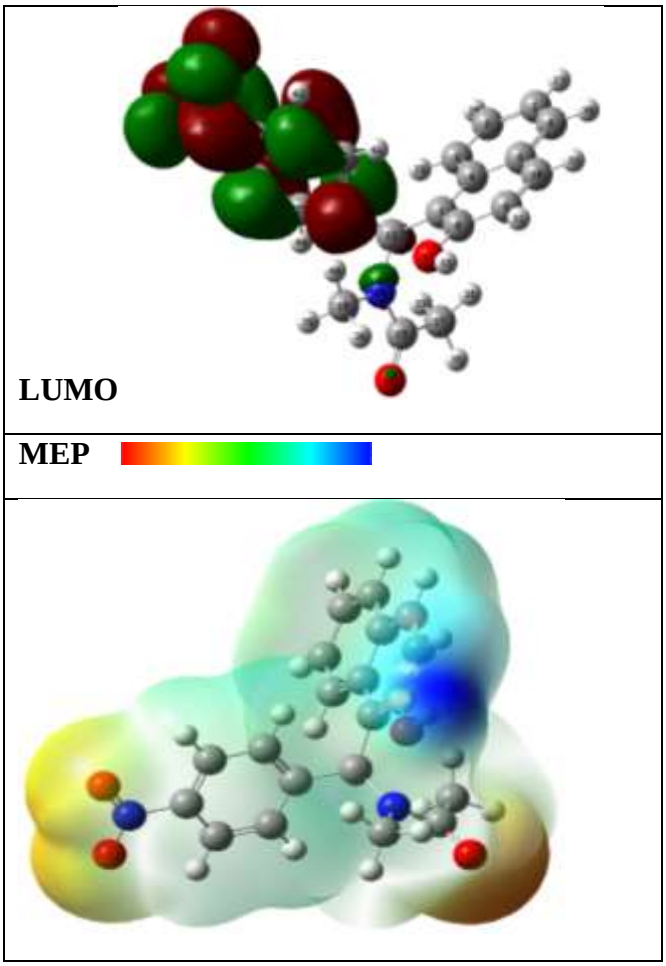

Figure 3: Frontier Molecular Orbitals (HOMO and LUMO) and MEP plots of HNMA.

3.6 Analysis of optical properties for HNMA based on UV-Visible spectrum

The provided UV-Visible spectrum of HNMA compound include both experimental and simulated (TD-DFT) data are given in Figure 4, offering insight into their electronic transitions and optical properties. The experimental spectra reveal that HNMA exhibit strong absorption in the UV region and the optical band gaps (E_g) are estimated as 3.51 eV. The spectral shapes indicate π-π^* electronic transitions, which are typical of conjugated aromatic systems.

The simulated spectra are obtained using TD-DFT with 6-31G (d,p) and 6-311G (d,p) basis sets. The computed band gaps for HNMA are 3.63 eV (6-31G (d,p)) and 3.52 eV (6-311G (d,p)), aligning well with experimental results. The spectral features indicate multiple electronic transitions, with HNMA showing an Intramolecular Charge Transfer (ICT) band, suggesting strong charge delocalization. The presence of an ICT band in HNMA implies stronger electron redistribution, which could impact charge transport efficiency in electronic applications. This study not only confirms the structure of HNMA, and high band gap of 3.511 eV, infer that it is transparent in visible region but primarily absorbs strongly in UV region.

3.7 Analysis of vibrational properties for HNMA based on Infrared Spectroscopy

Infrared (IR) spectroscopy is a powerful technique for investigating molecular vibrations and functional group interactions. The simulated (Figure 5) and experimental IR spectra of HNMA provide valuable insights into their structural and electronic properties. In the simulated spectra, HNMA exhibits a strong and broad hydroxyl (-OH) stretching absorption around 3600-3700 cm^{-1}, indicating intramolecular hydrogen bonding. The carbonyl (C=O) stretching appears near 1728 cm^{-1}, confirming the acetyl functional group. The nitro (-NO_2) asymmetric and symmetric stretching vibrations occur around 1340-1530 cm^{-1}, which is characteristic of HNMA. The aromatic and aliphatic C-H stretching vibrations are observed in the 3000-3100 cm^{-1} range, while the C-N stretching mode appears at 1200-1300 cm^{-1}, associated with the amide linkage and nitrogen-carbon interactions.

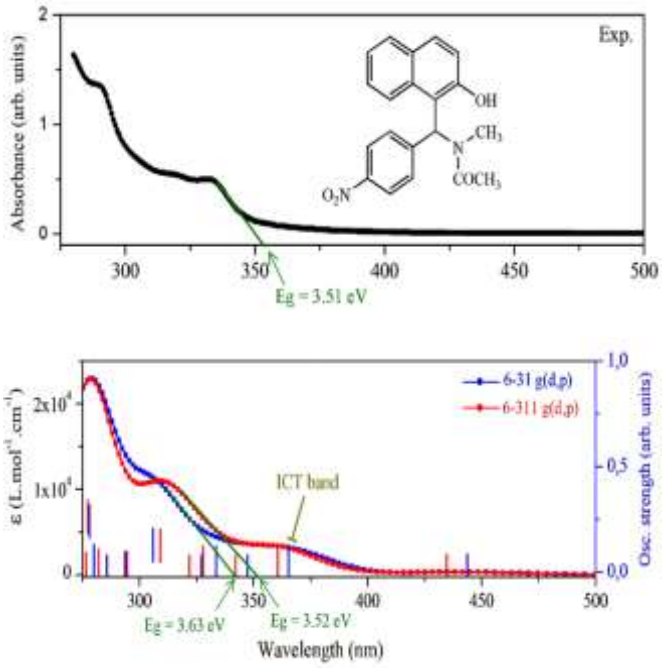

Figure 4: Experimental and simulated UV-Vis optical spectra of HNMA compound.

Comparison with experimental IR spectra reveals peak shifts and broadening due to solvent effects, intermolecular interactions, and anharmonicities. The hydroxyl (-OH) stretching band is broader and shifted to lower frequencies, indicating strong hydrogen bonding interactions. The carbonyl stretching appears at slightly lower wavenumbers (~1700 cm^{-1}) for HNMA, suggesting environmental stabilization. Experimental spectra exhibit variations in peak intensity due to differences in sample preparation and measurement conditions.

The vibrational analysis of HNMA using simulated and experimental IR spectra highlights the impact of structural modifications on molecular vibrations. Experimental spectra confirm theoretical predictions, with slight shifts due to hydrogen bonding and intermolecular interactions. These findings provide valuable insights into the structure-property relationships of HNMA, aiding in their characterization and potential applications in molecular design.

3.8 Raman Spectroscopic Analysis

The Raman spectrum of HNMA was simulated using Density Functional Theory (DFT) at the B3LYP/6-311G (d,p) level to analyze their vibrational characteristics. The spectral features highlight the influence of their distinct functional groups on vibrational modes.

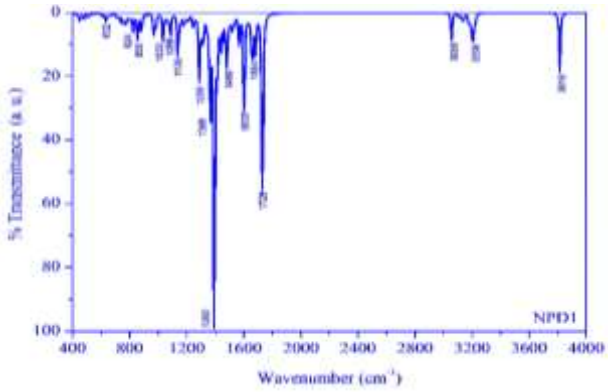

Figure 5: Simulated Infrared spectra of HNMA

It exhibits a strong Raman-active mode are observed at 1392 cm^{-1} (NO_2 symmetric stretching), 1656 cm^{-1} (C=C stretching), and 3200 cm^{-1} (O-H stretching). Additional peaks are identified at 1136 cm^{-1} (C-N stretching), 1480 cm^{-1} (aromatic ring stretching), 3056 cm^{-1} (C-H stretching), and 3816 cm^{-1} (high-frequency O-H stretching mode).

These results validate the use of Raman spectroscopy for structural characterization and confirm the computational approach's reliability in predicting vibrational properties. These details are shown in Figure 6.

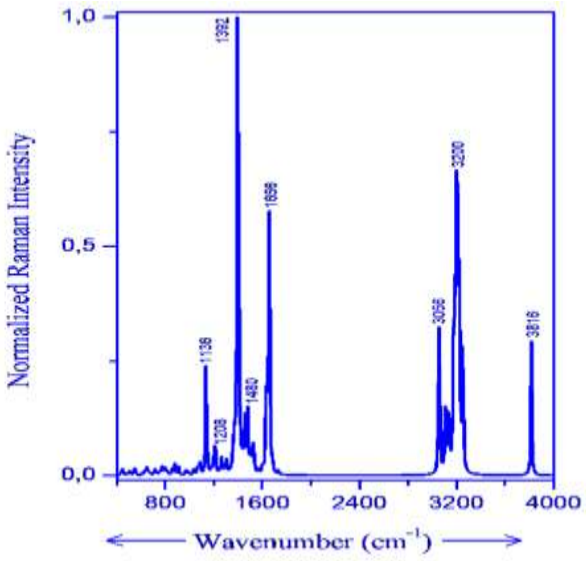

Figure 6: Simulated Raman spectra of HNMA.

3.9 Comprehensive NMR Analysis

The ^{1}H- and ^{13}C-NMR spectra of HNMA were thoroughly investigated by comparing experimentally measured chemical shifts with computationally predicted values. The high level of correlation between the two datasets confirms the structural integrity of the studied compounds and underscores the accuracy of the computational method employed.

^{1}H-NMR Analysis

The experimental ^{1}H chemical shifts for HNMA is in excellent agreement with the calculated values, with deviations primarily attributed to environmental effects such as solvent interactions, hydrogen bonding, and minor conformational variations. The aromatic proton region (7.0-8.5 ppm) is well-resolved, indicating π-electron delocalization and the presence of conjugated systems. In HNMA, the shifts at 8.081, 8.064, and 8.061 ppm (corresponding to 43-H, 42-H, and 32-H) are consistent with deshielded proton environments due to electron-withdrawing effects from adjacent functional groups.

^{13}C-NMR Analysis and Computational Validation

The ^{13}C chemical shifts provide critical insights into the electronic environment of the molecular framework. Carbonyl carbon atoms exhibit characteristic downfield shifts at 175.603 ppm indicative of strong electron-withdrawing effects. The aromatic carbons span 164.442-119.099 ppm, with slight deviations between calculated and experimental values arising from local electronic perturbations

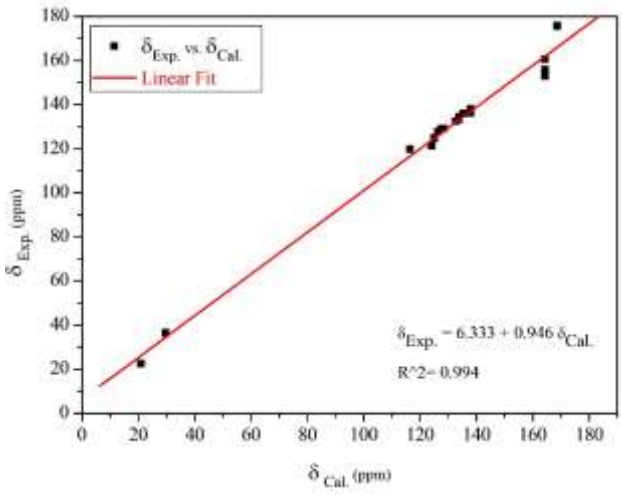

Figure 7: Relationship between experimental and computed ^{13}C chemical shifts (ppm) for HNMA

The remarkable agreement between experimental and calculated ^{1}H- and ^{13}C-NMR shifts confirms the structural assignments of HNMA, reinforcing the accuracy of the applied computational methodology (Figure 7). The slight deviations observed are well within expected tolerances and can be attributed to environmental factors. The high R^2 value (0.999) in the ^{13}C correlation plot further supports the predictive power of the theoretical approach, making it a reliable tool for future structural elucidation and NMR spectral assignments of related molecular systems.

3.10 Analysis of computed nonlinear optical (NLO) parameters

The NLO properties of the HNMA was evaluated by computing their dipole moment (μ), mean polarizability (α), and first-order hyperpolarizability (β) using the 6-31G(d,p) and 6-311G(d,p) basis sets. These parameters provide insight into the molecular charge distribution, electronic responsiveness, and potential applications in optoelectronic devices.

The dipole moment reflects the charge separation within a molecule, influencing its electrostatic interactions and alignment in external fields. It exhibits a higher dipole moment with values increasing slightly when using 6-311G (d,p) (from 7.029 D to 7.110 D). This suggests a greater degree of charge separation in HNMA, which is often, associated with enhanced intramolecular charge transfer (ICT) effects.

Polarizability quantifies the molecule's ability to distort under an applied electric field, influencing its refractive index and linear optical properties. Hyperpolarizability is a key parameter in second-order nonlinear optical effects such as second-harmonic generation (SHG) and electro-optic modulation. The results indicate that HNMA exhibits significantly higher β values, emphasizing its superior NLO potential. Using the 6-31G (d,p) basis set, HNMA has a β value of 2926.645 a.u., which remains nearly unchanged with 6-311G (d,p) (2911.570 a.u.). This suggest that HNMA is a much stronger candidate for NLO applications, likely due to more efficient charge transfer along its molecular backbone.

For efficient computational analysis, 6-31G (d,p) is suitable for preliminary studies, while 6-311G (d,p) provides a more precise representation of molecular polarizability. The NLO evaluations establish HNMA as the superior candidate, exhibiting a higher dipole moment, comparable polarizability, and significantly enhanced hyperpolarizability, making it more promising for advanced NLO applications. The values are depicted in Table 4.

Basis Set	Dipole Moment (Debye)	Polarizability (α, a.u)	Hyper-polarizability (β, a.u)
6-31g(d,p)	7.029	303.469	2926.645
6-311g(d,p)	7.110	322.435	2911.570

Table 4: Computed NLO parameters for investigated for HNMA.

3.11. Topological quantum theory of atoms in molecules (QTAIM) analysis

To provide clear insights into the types and nature of intra- and intermolecular interactions between atoms and groups within studied compounds, QTAIM analysis is a highly suitable method for addressing these concepts[39-42]. In the QTAIM method, bond critical points (BCPs) between two attractors (i.e., two atoms interacting or bonded) are meticulously examined. This theory posits that the value of electron density, the Laplacian of electron density, and other selected topological parameters yields valuable insights into the strength and the characteristic of bonds. Specifically, the negative and positive values of the $\nabla^2\rho_B$ correspond to covalent bonds and non-covalent interactions (such as H-bonds, van der Waals forces, steric effects, and ionic bonds). The topological parameters were generated using the Multiwfn package [43]. The QTAIM

graphs and topological parameters are presented in Figure 8 and Table 5. For HNMA, the $\rho_B/\nabla^2\rho_B$ values are 0.0132 a.u. /0.0484 a.u. (BCP1) and 0.0149 a.u. /0.0611 a.u. (BCP2), indicating the presence of non-covalent interactions among nitrogen (N), oxygen (O), and hydrogen (H) atoms. In these BCPs, the interaction energy ($V_B/2$) is approximately -13.65 kJ. mol^{-1} and -12.47 $kJ.mol^{-1}$, suggesting a good stability of the material. The ellipticity of electron density (ε_B) is measured at 0.016 and 0.31 a.u., further indicating the robustness stability of these interactions and enhancing the stability of HNMA. Additionally, Table 5 demonstrates that the $\frac{|V_B|}{G_B}$ ratio is less than unity, confirming that the interactions are non-covalent in nature (van der Waals forces).

B-S	$\rho_B/\nabla^2\rho_B$	V_B	G_B	$\frac{\lvert V_B \rvert}{G_B}$	$V_B/2$	ε_B
B_1	0.0132/ 0.0484	-0.0104	0.0113	0.92	-13.65	0.016
B_2	0.0149/ 0.0611	-0.0095	0.0124	0.76	-12.47	0.31

Table 5. QTAIM topological parameters (in a.u.) and the estimated binding energy $E_B = V_B/2$ in $kJ.mol^{-1}$at each binding site (B-S) of HNMA**.**

3.12. Non-covalent interaction (NCI) and reduced density gradient (RDG) analyses

To visualize the interaction between atoms, we can employ two extensions of QTAIM analysis (Figure 8), namely NCI (Figures 9) and RDG iso-surface (Figures 10)**.** The NCI plots were generated using the VMD program[44]. The RDG analysis is calculated using the following equation[45].

$$\mathbf{RDG} = \frac{\mathbf{1}}{\mathbf{2(2(3\pi^2)^{1/3}}} \frac{\boldsymbol{\nabla\rho(r)}}{\mathbf{(\rho(r))^{4/3}}}$$

The 2D-RDG plot provides insights into the nature of interactions, utilizing color codes to represent different types: hydrogen bonds are depicted in blue, van der Waals interactions in green and steric effects in red. Similarly, the NCI index employs colored disks situated between interacting atoms to illustrate these interactions. The NCI iso-surface reveals a green disk positioned between oxygen (O), hydrogen (H),

nitrogen (N), and carbon (C), indicating the presence of van der Waals interactions, specifically, O···N and H···H, H···N and H···C, thereby corroborating the result obtained by QTAIM analysis.

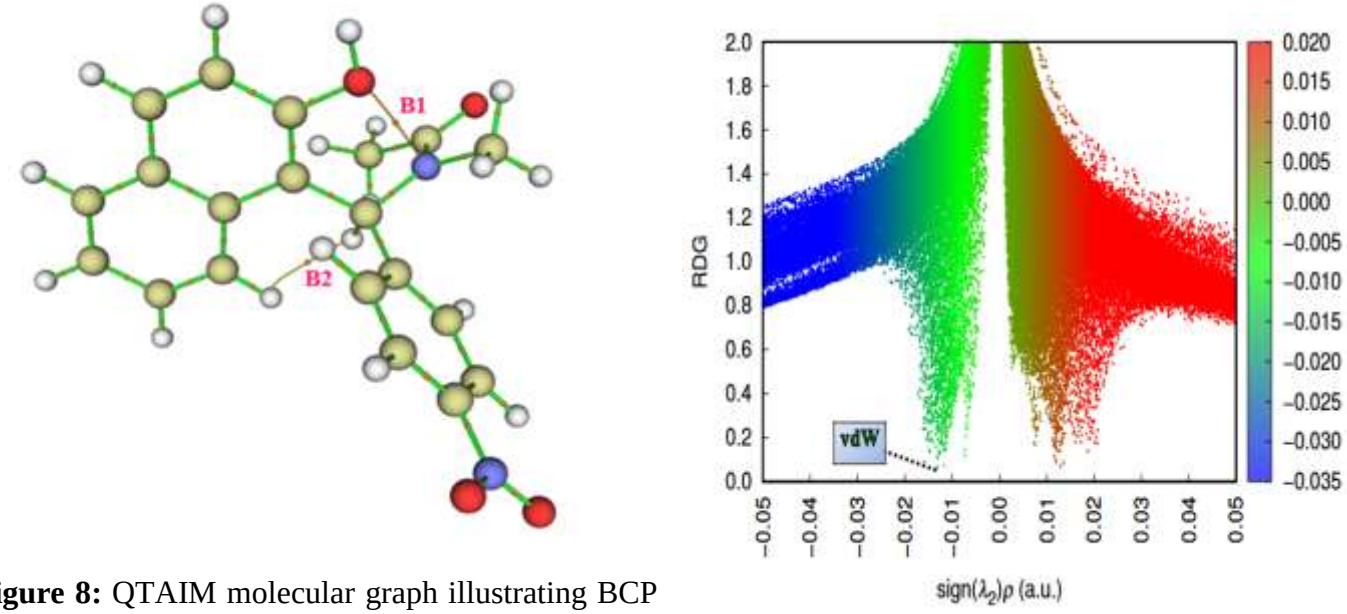

Figure 8: QTAIM molecular graph illustrating BCP characteristics for HNMA

Furthermore, the RDG plot displays (Figure 10) two picks for HNMA, oriented at approximately -0.015 a.u., which signifies the presence of vdW forces at these binding sites. Collectively, the NCI and RDG plots suggest that HNMA is significantly stabilized by several vdW interactions.

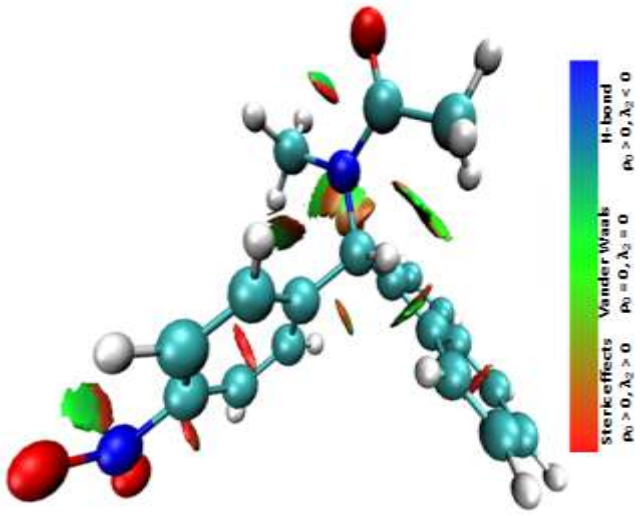

Figure 9: NCI plot of HNMA generated using the VMD program

3.13. Electron Localization Function (ELF) and Localized Orbital Locator (LOL) analyses

The ELF and LOL analyses offer profound electron localization and the charge transfer mechanism that occurs in the studied compounds[46,47]. These methodologies meticulously investigate the bonding, non-bonding interactions, and lone electron pairs at active sites. Furthermore, they facilitate the classification of chemical bonding, elucidate atomic shell structure, and validate charge

Figure 10: RDG plot of HNMA

bonding interactions. The ELF and LOL plots are quantified on scales ranging from 0 to 1 and 0 to 0.8, respectively. An ELF value exceeding 0.5 signifies the presence of localized bonding electrons, whereas a value below 0.5 indicates delocalized electrons. In the ELF plots for HNMA exhibits a pronounced dark red color is observed surrounding the hydrogen (H) atoms and –C-C bonding, while a blue color overlaps the carbons (C) and nitrogen (N) atoms. This representation signifies the presence of bonding and delocalization of electrons at these binding sites (ELF = 1). Such a finding suggests a potential electronic charge transfer (ECT) across the surface of the compounds, thereby facilitating electrostatic interactions that enhance their stability. Furthermore, these results indicate the presence of several donor-acceptor groups within the compound, ensuring well atomic organization, which is advantageous for sensor and biological applications. The 2D-LOL iso-surface further corroborates the ELF results. These details are given Figure 11.

3.14 Docking study of HNMA with HIV-1 protein

The docking analysis was conducted to investigate their interactions with the target protein 1PVG, which is associated with HIV-1. The binding affinities and crucial interactions observed provide insights into the compound's potential as therapeutic agents. Figure 12 demonstrated a significant binding interaction with TYR-245 residue at a distance of 2.5 Å, showing a stable hydrogen bonding pattern. The docking score for this compound was -7.8 kcal/mol, indicating a favourable binding interaction. The docking poses reveal that HNMA interact with key residues within the binding sites of HIV-1 protease, suggesting the formation of stable ligand-protein complexes. The interactions observed for HNMA involve hydrogen bonding and π-π stacking, contributing to enhanced stability and binding efficiency. Thus HNMA hold potential as lead molecules for further optimization and development as potential inhibitors for HIV-1 protease. The interaction with residue TYR-245 suggest that this site may be critical for ligand binding and could be targeted in subsequent drug design efforts.

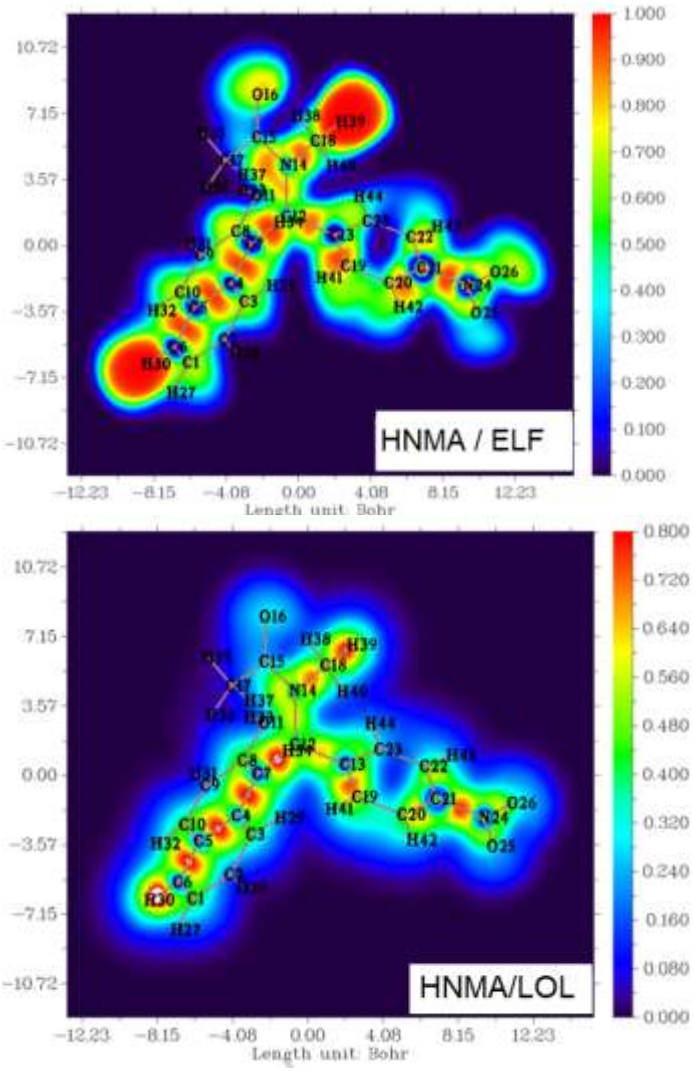

Figure 11: 2D-ELF and 2D-LOL plots of HNMA

4. CONCLUSION

In this work, we describe an efficient strategy for the synthesis of naphthol derivative HNMA by making use of TCA as well as montmorillonite K10 clay as catalyst, which were characterized by FT-IR and H^1 & ^{13}C NMR and QTOF mass spectral studies. The yield of the compounds prepared was found to be better using TCA compared with conventional montmorillonite K10 clay. Thus, synthesized HNMA possess antibacterial activity under *in vitro* studies against pathogenic bacteria's namely Escherichia coli and Staphylococcus aureus.

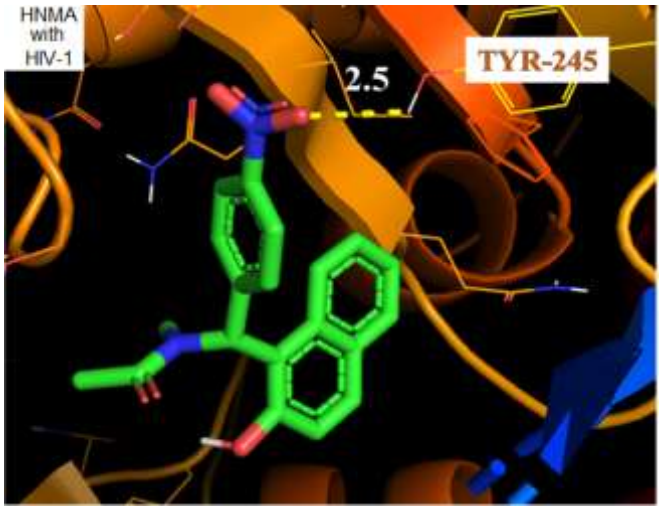

Figure 12: Docking interaction of HNMA against HIV-1 protein (1PVG).

Additionally, HNMA exhibit excellent antioxidant properties too. The results of this work are complemented and discussed within the scope of quantum chemical calculations with DFT calculations. The MEP map shows that HNMA has stronger affinity towards nucleophiles. The high band gap value obtained from UV-Visible spectrum suggest, it is transparent in visible region. Vibrational analysis from IR and Raman spectrum further confirms structure of HNMA. QTAIM analysis suggest, the interactions between atoms and groups with in the HNMA structure is non-covalent in nature. Docking analysis of HNMA against HIV-1 protein reveal that the residue TYR-245 site may be critical for ligand binding and could be targeted in subsequent drug design efforts. So, we conclude that HNMA has interesting potential applications and enlighten further research areas.

REFERENCES

[1] J. Zhu, H. Bienayme (Eds.), *Multi component Reactions*, Wiley- VCH, Weinheim, **2005**.
[2] A. Domling, I. Ugi, Angew. Chem., Int. Ed. 39 (2000) 3168; (b) I. Ugi, B. Werner, A. Domling, *Molecules*, 8, **2003**, 53.
[3] L. Banfi, R. Riva, The Passerini Reaction, in: L.E. Overman (Ed.), *Organic Reactions*, 65, Wiley, Hoboken, New Jersey (USA), **2005**, 1.
[4] L.E. Overman, D.J. Ricca, The Intramolecular Mannich and Related Reactions, in: B.M. Trost, I. Fleming (Eds.), *Comprehensive Organic Synthesis*, 2, Pergamon Press, Oxford, **1991**, 1007.
[5] Zhu J, Bienayme H (Eds): *Multicomponent Reactions*. **2005**
[6] Shi, D.; Mou, J.; Zhuang, Q.; Niu, L.; Wu, N.; Wang, X. Three-component one-pot synthesis of 1,4-dihydropyrano[2,3- c]pyrazole derivativesin aqueous media. *Synth. Commun*. **2004**, 34, 4557 – 4563.
[7] Jin, T. S.; Wang, A. Q.; Cheng, Z. L.; Zhang, J.-S.; Li, T. S. A clean and simple synthesis of 6-amino-4-aryl-5-cyano-3-methyl-1-phenyl-1,4- dihydropyrano[2,3- c]pyrazole in water. *Synth. Commun*. **2005**, 35, 137 – 143.
[8] Jin, T. S.; Zhao, R. Q.; Li, T. S. 14. A one-pot three-component process for the synthesis of amino-4-aryl-5-cyano-3-methyl-1-phenyl-1,4-dihydropyrano [2,3- c] pyrazoles in aqueous media. *ARKIVOC*, **2006**, xi, 176 – 182.

[9] Heravi, M. M.; Ghods, A.; Derikvand, F.; Bakhtiari, K.; Bamoharram, F. F. H_{14} [NaP_5 W_{30} O_{110}] catalyzed one-pot three-component synthesis of dihydropyrano [2,3- c] pyrazole and pyrano [2,3- d] pyrimidine derivatives. *J. Iran Chem. Soc.* **2010**, 7, 615 – 620.
[10] Khurana, J. M.; Nand, B.; Kumar, S. Rapid synthesis of polyfunctionalized pyrano [2,3- c] pyrazoles via multicomponent condensation in room-temperature ionic liquids. *Synth. Commun*. **2011**, 41, 405 – 410.
[11] Kshirsagar, S. W.; Patil, N. R.; Samant, S. D. Mg-Al hydrotalcite as a first heterogeneous basic catalyst for the synthesis of 4h-pyrano [2,3- c] pyrazoles through a four-component reaction. *Synth. Commun.* **2011**, 41, 1320 – 1325.
[12] Kumar, B.S.; Dhakshinamoorthy, A.; Pitchumani, K. K10 montmorillonite clays as environmentally benign catalysts for organic reactions. *Catal. Sci. Technol.* **2014**, *4*, 2378–2396.
[13] Hechelski, M.; Ghinet, A.; Brice Louvel, B.; Dufrenoy, P.; Rigo, B.; Daïch, A.; Waterlot, C. From Conventional Lewis Acids to Heterogeneous Montmorillonite K10: Eco-Friendly Plant-Based Catalysts Used as Green Lewis Acids. *Chem.Sus.Chem* **2018**, *11*, 1249–1277.
[14] Hashemi, M.M.; Eftekhari-Sis, B.; Abdollahifar, A.; Khalili, B. ZrOCl2·8H2O on montmorillonite K10 accelerated conjugate addition of amines to α, β-unsaturated alkenes under solvent-free conditions. *Tetrahedron* **2006**, *62*, 672–677.
[15] Bonacci, S.; Nardi, M.; Costanzo, P.; De Nino, A.; Di Gioia, M.L.; Oliverio, M.; Procopio, A. Montmorillonite K10-Catalyzed Solvent-Free Conversion of Furfural into Cyclopentenones. *Catalysts,* **2019**, *9*(3), 301.
[16] Z. Karimi-Jaberi and M. M. Reyazo Shams, "Trichloroacetic acid as a solid heterogeneous catalyst for the rapid synthesis of dihydropyrano[2,3-c]pyrazoles under solvent-free conditions,"*Heterocyclic Comm.*, vol. 17, 5-6, 177–179, **2011**.
[17] Z. Karimi-Jaberi, S. Z. Abbasi, B. Pooladian, and M. Jokar, "Efficient, one-pot synthesis of tetrahydrobenzo[*a*]xanthen-11- ones and dibenzo[a,j]xanthenes using trichloroacetic acid as a solid heterogeneous catalyst under solvent-free conditions," *E. Journal of Chemistry*, vol. 8, no. 4, pp. 1895–1899, **2011**.
[18] Z. Karimi-Jaberi and B. Pooladian, "A facile synthesis of new 2-amino-4 h -pyran-3-carbonitriles by a one-pot reaction of *αα*, *αα*'-Bis(arylidene) cycloalkanones and malononitrile in the presence of K_2CO_3," *The Scientific World Journal*, vol. **2012**.
[19] Z. Karimi-Jaberi and B. Pooladian, "A facile synthesis of *α*,'- bis(substituted benzylidene) cycloalkanones catalyzed by p- TSA under solvent-free conditions," *Green Chemistry Letters and Reviews*, vol. 5, 2, 187–193, **2012**.
[20] Martelli G., Giacomini D. Antibacterial and antioxidant activities for natural and synthetic dual-active compounds. *Eur. J. Med. Chem.* **2018**; 158:91–105.
[21] Kim S.Y., Park C., Jang H.-J., Kim B.-o., Bae H.-W., Chung I.-Y., Kim E.S., Cho Y.-H. Antibacterial strategies inspired by oxidative stress and response networks. *J. Microbiol.,* **2019**; 57:203–212.
[22] Rios JL Recio MC, Villar A. Screening methods for natural products with antimicrobial activity: A review of the literature. *J Ethnopharmacol.* **1988**; 23:127–49.
[23] Alzoreky NS, Nakahara K. Antibacterial activity of extracts from some edible plants commonly consumed in Asia. *Int J Food Microbiol.*, **2003**; 80:223–30.
[24] Bauer AW, Kirby WMM, Sherris JC, Turck M. Antibiotic susceptibility testing by standardized single disc method. *Am J ClinPathol.* **1966**; 36:493–6.
[25] Katalinic V., Milos M., Kulisic T., Jukic M. Screening of 70 medicinal plant extracts for antioxidant capacity and total phenols. *Food Chem*. **2006**; 94:550–557.

[26] Frisch M.J. et al., *Gaussian 09 Revision C01. Gaussian*, Inc. Wallingford. **2009**.
[27] Dennington R., Keith T., Millam A., John M., *Semichem Inc.*, Shawnee Mission, KS, **2009**.
[28] T. Lu, F. Chen, Multiwfn: A multifunctional wavefunction analyzer, *J. Comp. Chem*. 33, **2012**, 580–592.
[29] B. Gassoumi, A.M. Ahmed Mahmoud, S. Nasr, A. Karayel, S. Özkınalı, M.E. Castro, F.J. Melendez, M. Mahdouani, L. Nouar, F. Madi, H. Ghalla, R. Bourguiga, R. Ben Chaabane, Y. Zhou, Revealing the effect of Co/Cu (d7/d9) cationic doping on an electronic acceptor ZnOnanocage surface for the adsorption of citric acid, vinyl alcohol, and sulfamethoxazole ligands: DFT-D3, QTAIM, IGM-NCI, and MD analysis, *Materials Chemistry and Physics*, 309, **2023**, 128364.
[30] B. Silvi, A. Savin, Classification of chemical bonds based on topological analysis of electron localization functions, *Nature*, **371** (1994) 683–686.
[31] I. Cherif, H. Raissi, K. Abiedh, B. Gassoumi, M. Teresa Caccamo, S. Magazù, A.H. Said, H. Fredj, B. Taoufik, S. Ayachi, Optoelectronic Properties and Nonlinear Optical Responses of Para-Substituted Nitrobenzofurazan Compound: *Insight into DFT Investigation and Experiment*, **2023**.
[32] Carla Bassarello, Paola Cimino, Luigi Gomez-Paloma, Raffaele Riccio, Giuseppe Bifulco, Simulation of 2D 1H homo- and 1H–13C heteronuclear NMR spectra of organic molecules by DFT calculations of spin–spin coupling constants and 1H and 13C-chemical shifts, *Tetrahedron*, 59, Issue 48, **2003**, 9555-9562.
[33] Tamer, O., Avcı, D., Çelikoğlu, E., Idil, O. & Atalay, Y. Crystal growth, structural and spectroscopic characterization, antimicrobial activity, DNA cleavage, molecular docking and density functional theory calculations of Zn (II) complex with 2-pyridinecarboxylic acid. *Appl. Organomet. Chem*. 32, e4540, **2018**.
[34] Nayan R. Bhalodia and V. J. Shukla, Antibacterial and antifungal activities from leaf extracts of Cassia fistula l.: An ethnomedicinal plant, *J Adv Pharm Technol Res*. **2011**, Apr-Jun; 2(2): 104–109.
[35] Dávalos A., Gómez-Cordovés C., Bartolomé B. Commercial Dietary Antioxidant Supplements Assayed for Their Antioxidant Activity by Different Methodologies. *J. Agric. Food Chem.*; 51:2512–2519, **2003**.
[36] Moon J.-K., Shibamoto T. Antioxidant assays for plant and food components. *J. Agric. Food Chem.*; 57:1655–1666, **2009**.
[37] Li Y., Xu L., and Guo S., Effects of solid-state fermentation with the Ganoderma spp. and Coriolus versicolor on the total phenol contents and antioxidant properties on black soybean, *Journal of Chemistry*. 8, 9462748, **2023**.
[38] Blois, M.S. (1958) Antioxidant Determinations by the Use of a Stable Free Radical. *Nature*, 181, 1199-1200.
[39] C.H. Belgacem, N. Missaoui, M.A.H. Khalafalla, G. Bouzid, H. Kahri, A.H. Bashal, A. Dhahri, L. Nouar, F.J. Melendez, M.E. Castro, H. Ghalla, Y. Zhou, Synthesis of ultramicroporouszeoliticimidazolate framework ZIF-8 via solid-state method using a minimum amount of deionized water for high greenhouse gas adsorption: A computational modelling, *J Environmental Chemical Engineering*, 12, **2024**, 112086.
[40] I. Chérif, H. Raissi, K. Abiedh, B. Gassoumi, M.T. Caccamo, S. Magazu, A.H. Said, F. Hassen, T. Boubaker, S. Ayachi, Exploration of intramolecular charge transfer in para-substituted nitrobenzofurazan: Experimental and theoretical analyses, SpectrochimicaActa Part A: *Molecular and Biomolecular Spectroscopy*, 301, **2023**, 122939.
[41] H. Hadi, G. Bouzid, S. Nasr, H. Ghalla, R. Ben Chaabane, S. Ayachi, Design, synthesis, and density functional theory studies of a new selective chemosensor for Pb2+, *HELIYON*, 9, **2023**, e20206.

[42] B. Gassoumi, N.A. Dlala, M. Echabaane, H. Ghalla, Y. Zhou, M.E. Castro, F.J. Melendez, N. Leila, F. Madi, R.B. Chaabane, Adsorption of toxic and non-toxic metals with the new model of CX[4]: Experimental and computational investigation, Spectroscopic, QTAIM, and Antibacterial activity analyses, *Journal of Molecular Structure* 1268, **2022**, 133618.

[43] T. Lu, F. Chen, Multiwfn: A multifunctional wavefunction analyzer, *Journal of Computational Chemistry*, **33,** 2012, 580–592.

[44] B. Gassoumi, A.M. Ahmed Mahmoud, S. Nasr, A. Karayel, S. Özkınalı, M.E. Castro, F.J. Melendez, Mahdouani, L. Nouar, F. Madi, H. Ghalla, R. Bourguiga, R. Ben Chaabane, Y. Zhou, Revealing the effect of Co/Cu (d7/d9) cationic doping on an electronic acceptor ZnOnanocage surface for the adsorption of citric acid, vinyl alcohol, and sulfamethoxazole ligands: DFT-D3, QTAIM, IGM-NCI, and MD analysis, *Materials Chemistry and Physics*, 309, **2023**, 128364.

[45] M. Harzallah, M. Medimagh, N. Issaoui, T. Roisnel, A. Brahim, Synthesis, X-ray crystal structure, Hirshfeld surface analysis, DFT, AIM, ELF, RDG and molecular docking studies of bis[4-(dimethylamino)pyridinium]di-μ-chlorido-bis[dichloridomercurate(II)], *Journal of Coordination Chemistry*, 74, **2021**, 2927–2946.

[46] Silvi, B.; Savin, A. "Classification of chemical bonds based on topological analysis of electron localization functions". *Nature*. 371, 6499, 683–686, **1994**.

[47] Sheryl Cherian Parakkal, Riya Datta, S. Muthu, Abdulaziz A. Al-Saadi, Structure of molecule, density gradient, orbital locator and reactivity of 5,6-dichloro-1-cyclopentyl-2-(methylsulfinyl)-1H-benzimidazole-potent inhibitor of map kinase, *Journal of Molecular Structure*, Volume 1289, **2023**, 135794.